FEM-based approaches for modeling of the resource-demanding magnetization problems with magnetic scalar potential

Alexander Chervyakov, JINR, Dubna

Abstract

Despite the excellent quality of numerical calculations, 3D FEA analysis based on the magnetic vector potential is computationally expensive and therefore limited by the available hardware resources for magnetostatic problems with complicated model geometries, large nonconducting regions, nonlinear materials and increased requirements for accuracy of calculations. To improve the computational efficiency of finite-element modeling for such problems, we propose therefore to use instead of vector the total scalar potential either in the combination with vector potential, or even separately. In the former case, both potentials are defined by Maxwell's equations for conducting and nonconducting regions of the problem domain and coupled together on their common interfacing boundaries. Thin cuts with the potential jumps are constructed in the current-free regions to make them simply connected and ensure the consistency of the vector-scalar formulation. In the latter case, the scalar potential is only defined for nonconducting regions, while the impact of inductors on the entire problem domain is modeled either with the help of the potential jumps across thin cuts, or by using the magnetization of linear and nonlinear permanent magnets. The comparative analysis of the numerical efficiency of proposed methods is carried out by using the model of the dipole magnet as an example. Most efficiently, these methods can be applied for modeling of the magnetic systems, where a significant number of simulations with significant variation in geometric shapes is required during development of the optimal system design.

SC dipole magnet

Modeling requirements

- B cyclic azimuthally on IER
- B growing radially on IER

precision 1 Gauss (10^{-4} Tesla) for field on median plane

many runs with many geometry changes are needed for developing the optimal system design

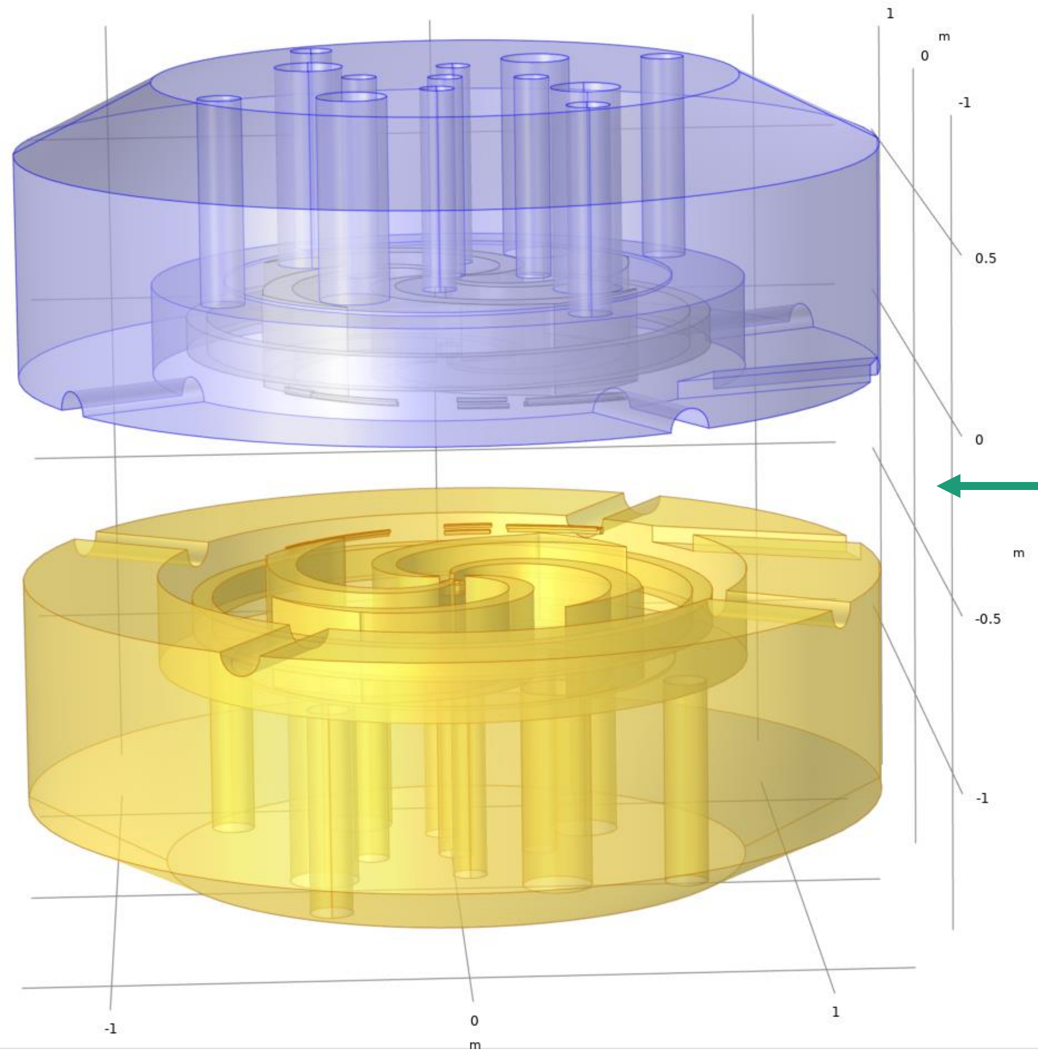

Injection & Extraction Region (IER)

How it works

B bends the path of charged particle

E accelerates the charge at each gap crossing

$$\boldsymbol{F} = q(\boldsymbol{E} + \boldsymbol{v} \times \boldsymbol{B})$$

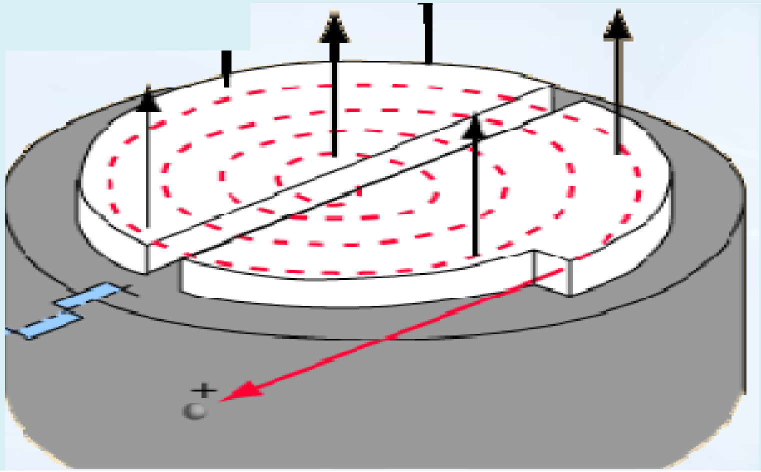

- Acceleration: $f_{RF} = h \cdot 2\pi\omega$
- Isochronism: mass increase is compensated by increase of B with radius
- Edge (Thomas) and spiral focusing
- Operation away from betatronic resonances

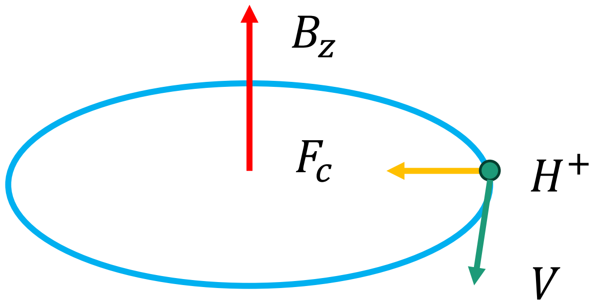

$$\omega = \frac{qB}{m}\ [radians/s]$$

Basic equations of computational magnetostatics

Ampere's law ($\nabla \cdot \boldsymbol{j} = 0$):

$$\nabla \times \boldsymbol{H} = \boldsymbol{j}, \qquad in \;\; \Omega, \tag{1}$$

Gauss's law:

$$\nabla \cdot \boldsymbol{B} = 0, \qquad in \;\; \Omega, \tag{2}$$

Material Law:

$$\boldsymbol{B} = \mu(H)\boldsymbol{H}, \qquad in \;\; \Omega, \tag{3}$$

$\mu(H)$ specified for each material, highly nonlinear for ferrites, discontinues across interfaces of different materials.

Boundary/Interface/symmetry conditions:

$$\boldsymbol{n} \times \boldsymbol{H} = \boldsymbol{0}, \qquad on \; \Gamma_h, \tag{4}$$

$$\boldsymbol{n} \cdot \boldsymbol{B} = 0. \qquad on \; \Gamma_b, \tag{5}$$

with $\Gamma = \partial\Omega = \Gamma_h \cup \Gamma_b$.

The first order div-curl system (1)-(3) consists of four scalar equations in three unknowns.

Magnetic vector potential: $\boldsymbol{B} = \boldsymbol{\nabla} \times \boldsymbol{A}$

Ampere's law:

$$\boldsymbol{\nabla} \times \left({}^{1}/_{\mu}\, \boldsymbol{\nabla} \times \boldsymbol{A}\right) = \boldsymbol{j} + \boldsymbol{\nabla}\psi, \qquad in\ \Omega, \tag{6}$$

where the Lagrange multiplier ψ uses to clean the divergence of $\boldsymbol{j}$ and to impose Coulomb gauge:

$$\boldsymbol{\nabla} \cdot \boldsymbol{A} = 0, \qquad in\ \Omega \tag{7}$$

Boundary conditions:

$$\boldsymbol{n} \times \boldsymbol{\nabla} \times \boldsymbol{A} = \boldsymbol{0}, \qquad on\ \Gamma_h, \tag{8}$$

$$\boldsymbol{n} \times \boldsymbol{A} = \boldsymbol{0}, \qquad on\ \Gamma_b, \tag{9}$$

MVP formulation is a standard tool providing excellent quality of calculation. However, using the potential $\boldsymbol{A}$ for the whole problem domain Ω is computationally demanding because of high memory consumption (direct solvers) and long processing time (iterative solvers).

Combining vector and scalar potentials

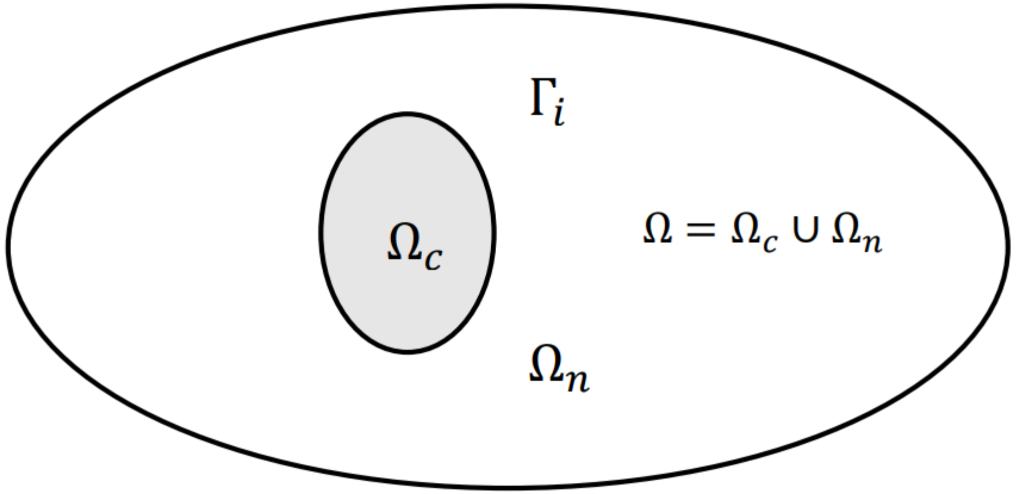

Figure 1: Typical computational domain of the magnetostatic problem.

Total scalar potential ($\boldsymbol{j} = 0$): $\boldsymbol{H} = -\nabla V_m$

Magnetic Gauss's law:

$$\nabla \cdot (\mu \nabla V_m) = 0, \qquad in \ \Omega, \tag{10}$$

Boundary condition:

$$V_m = 0, \qquad on\, \Gamma_h, \tag{11}$$

$$\boldsymbol{n} \cdot \nabla V_m = 0, \qquad on\, \Gamma_b. \tag{12}$$

Making Ω_n simply connected:

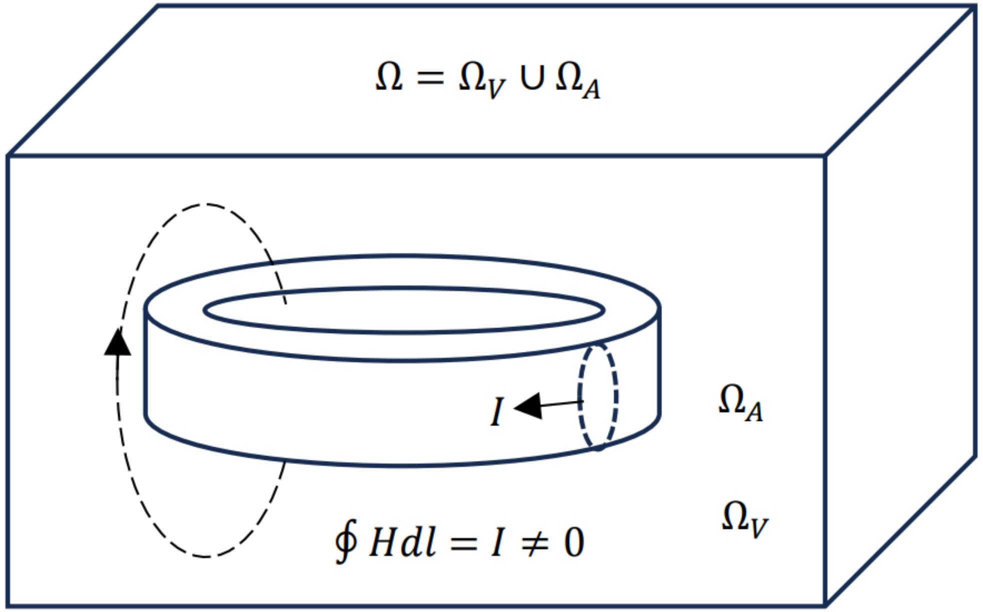

Figure 2:Typical non-conducting multiply connected region Ω_V

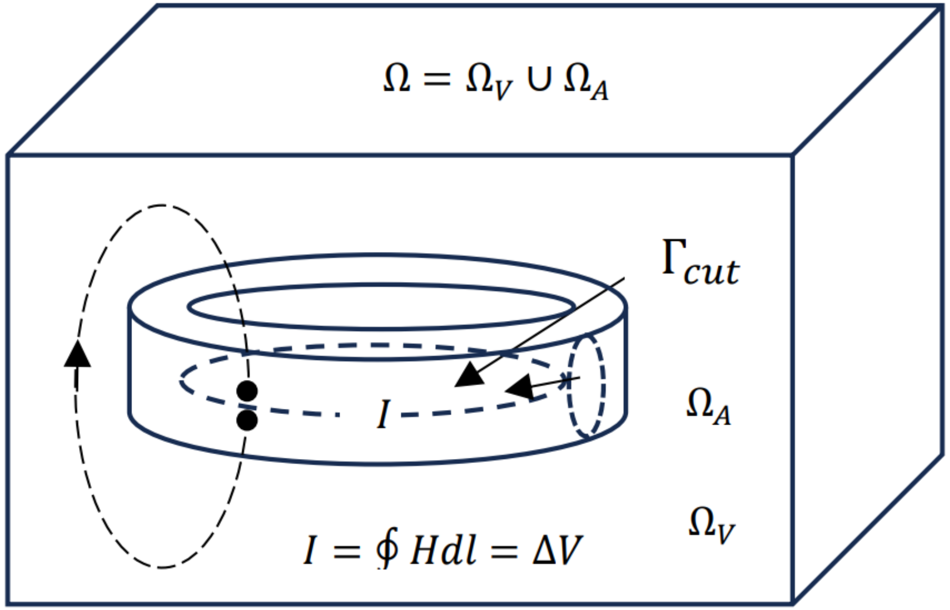

Figure 3: Thin cut plane with the potential discontinuity.

The potential discontinuity is given by Ampere's law:

$$\Delta V_m = V_m^+ - V_m^- = I, \qquad on\ \Gamma_{cut}. \tag{13}$$

Position and form of the cut surface and potentials coupling:

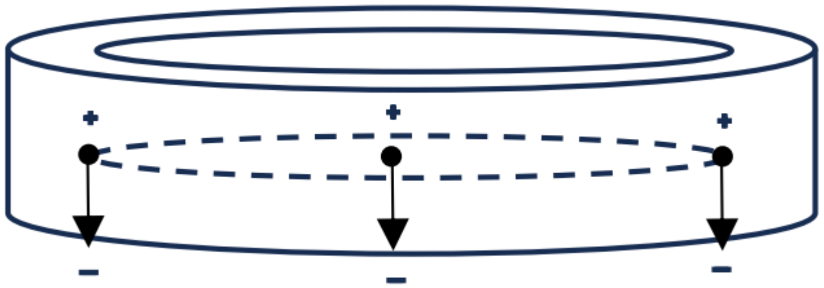

Figure 4: All positions of the cut plane fully preventing any closed loop from linking the current are equally good.

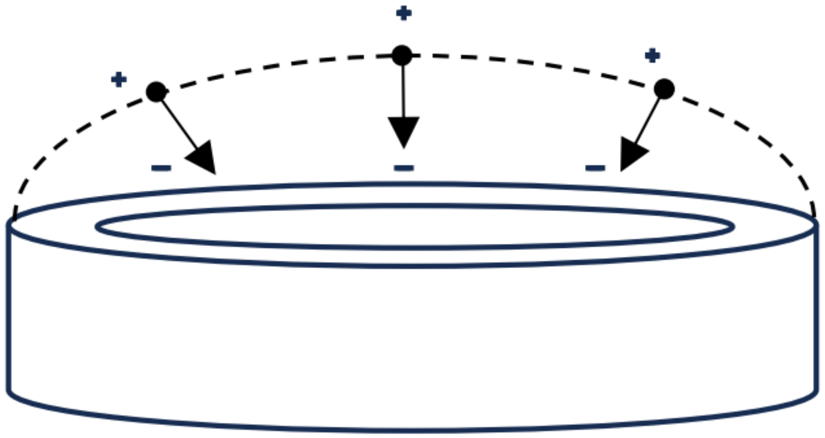

Figure 5: The form of the cut surface defines the directions of the potential jump.

Both potentials should be coupled on their common interfacing boundary Γ_i:

$$(1/\mu_c) \cdot \boldsymbol{n} \times (\boldsymbol{\nabla} \times \boldsymbol{A}) = -\,\boldsymbol{n} \times \boldsymbol{\nabla} \cdot V_m, \qquad on\ \Gamma_i, \tag{14}$$

$$-\,\mu_n \cdot \boldsymbol{n} \cdot \boldsymbol{\nabla} \cdot V_m = \boldsymbol{n} \cdot (\boldsymbol{\nabla} \times \boldsymbol{A}), \qquad on\ \Gamma_i, \tag{15}$$

FEM method: converting into weak integral form

MVP formulation for entire domain Ω ($\boldsymbol{j} \neq \mathbf{0}$):

$$\int_\Omega \left({}^1\!/_\mu\, \nabla \times \boldsymbol{A}\right) \cdot (\nabla \times \boldsymbol{w}) dv = \int_\Omega \boldsymbol{j} \cdot \boldsymbol{w}\, dv + \int_\Omega (\nabla\psi) \cdot \boldsymbol{w} dv\,, \qquad (16)$$

$$\int_\Omega \boldsymbol{A} \cdot (\nabla\zeta) dv = 0, \qquad (17)$$

with $\zeta = 0$ and $\boldsymbol{n} \times \boldsymbol{w} = \mathbf{0}, on\ \Gamma_b$.

MSP formulation with/without single cut for entire domain Ω ($\boldsymbol{j} = \mathbf{0}$):

$$\int_\Omega (\mu \nabla V_m) \cdot (\nabla\zeta) dv - \int_{\Gamma_{cut}} \mu\zeta \boldsymbol{n} \cdot (\nabla V_m^+ - \nabla V_m^-) ds = 0\,, \qquad (18)$$

with $\zeta = 0\ on\ \Gamma_h$.

FEM method: converting into weak integral form

MVP&MSP formulation for $\Omega = \Omega_c \cup \Omega_n$:

$$\int_{\Omega_c} \left({}^{1}/_{\mu_c}\ \nabla \times \boldsymbol{A}\right) \cdot (\nabla \times \boldsymbol{w}) dv - \int_{\Gamma_i} (\boldsymbol{n} \times \nabla V_m) \cdot \boldsymbol{w} ds = \int_{\Omega_c} \boldsymbol{j} \cdot \boldsymbol{w}\, dv + \int_{\Omega_c} (\nabla \psi) \cdot \boldsymbol{w}\, dv, \qquad (19)$$

$$\int_{\Omega_n} (\mu_n \nabla V_m) \cdot (\nabla \zeta) dv + \int_{\Gamma_i} \boldsymbol{n} \cdot (\nabla \times \boldsymbol{A}) \zeta ds - \int_{\Gamma_{cut}} \mu_n \zeta \boldsymbol{n} \cdot (\nabla V_m^{+} - \nabla V_m^{-}) ds = 0\,, \qquad (20)$$

$$\int_{\Omega_c} \boldsymbol{A} \cdot (\nabla \xi) dv = 0, \qquad (21)$$

FEM method: meshing and approximating

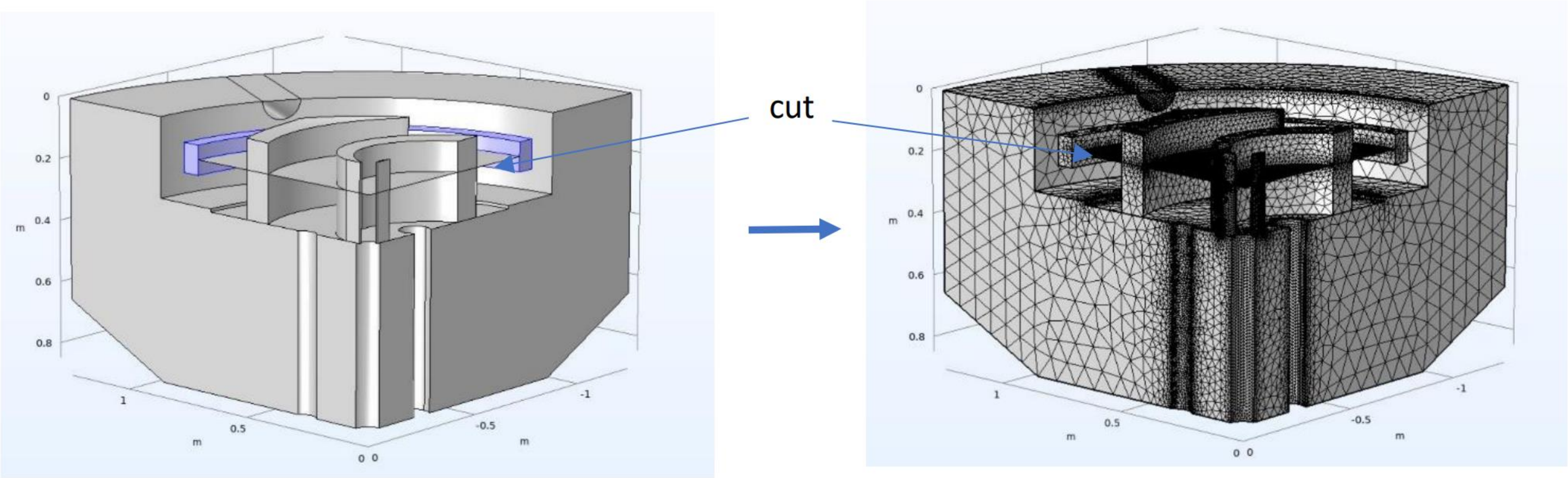

Figure 6: The finite-element mesh for 1/8-th part of the geometry of dipole magnet.

$$\boldsymbol{A} \approx \sum_{i=1}^{k} a_i \cdot \boldsymbol{w_i} \qquad V_m \approx \sum_{i=1}^{n} v_i \cdot \zeta_i \tag{22}$$

DOFs

$\boldsymbol{w}_i$ - edge shape functions

ζ_i - nodal shape functions

k - number of edges

n - number of nodes

FEM method: discretizing with Galerkin method

$$\begin{bmatrix} A & C \\ -C^T & B \end{bmatrix} \begin{pmatrix} a \\ v \end{pmatrix} = \begin{pmatrix} f \\ 0 \end{pmatrix} \tag{23}$$

with

$$A_{ij} = \int_{\Omega_c} \left({}^1/_{\mu_c} \, \boldsymbol{\nabla} \times \boldsymbol{w}_i \right) \cdot (\boldsymbol{\nabla} \times \boldsymbol{w}_j) dv \tag{24}$$

$$B_{ij} = \int_{\Omega_n} (\mu_n \boldsymbol{\nabla} \zeta_i) \cdot (\boldsymbol{\nabla} \zeta_j) dv + \int_{\Gamma_{cut}} \mu_n \boldsymbol{n} \cdot \boldsymbol{\nabla}(\Delta\zeta_i)\zeta_j ds \tag{25}$$

$$\Delta\zeta_i \equiv \zeta_i^+ - \zeta_i^-$$

$$C_{ij} = \int_{\Gamma_i} (\boldsymbol{\nabla}\zeta_{\boldsymbol{i}} \times \boldsymbol{n}) \cdot \boldsymbol{w}_j ds \tag{26}$$

$$f_i = \int_{\Omega_c} \boldsymbol{j} \cdot \boldsymbol{w}_i \, dv + \int_{\Omega_c} (\boldsymbol{\nabla}\psi) \cdot \boldsymbol{w}_i \, dv \tag{27}$$

$$K \cdot a = 0 \tag{28}$$

with

$$K_{ij} = \int_{\Omega_c} \boldsymbol{w}_i \cdot (\boldsymbol{\nabla}\xi_j) dv \tag{29}$$

FEM method: assembling and solving

- Fully coupled approach
- Newton's type methods for nonlinear solver
- Direct multifrontal Pardiso solver
- Lower-upper triangular decomposition

$$A \cdot x = b \quad \longrightarrow \quad \begin{aligned} A &= L \cdot U \\ x &= U^{-1} \cdot y \\ y &= L^{-1} \cdot b \end{aligned}$$

Solution:

Chervyakov A., On the use of mixed potential formulation for finite-element analysis of large-scale magnetization problems with large memory demand//arXiv:2307.12308v1[physics. comp-ph] 2023;
Chervyakov A.M., On finite-element modeling of large-scale magnetization problems with combined magnetic vector and scalar potentials//preprint JINR E11-2023-37, 2023.

FEM solver available:

Degrees of freedom (DOF) N versus Computational Resources

SLAE $\boldsymbol{A \cdot x = b}$

Direct solvers	2D	3D
Memory	$\mathcal{O}(N \log N)$	$\mathcal{O}(N^{4/3})$
Time	$\mathcal{O}(N^{3/2})$	$\mathcal{O}(N^2)$

Intel® PARDISO (fastest), MUMPS, Dense Matrix Solver, SPOOLES (slowest)

LU decomposition $A = LU, \quad L(U \cdot x) = L \cdot y = b$

Direct substitution $y = L^{-1} \cdot b$

Inverse substitution $x = U^{-1} \cdot y$

Pros: stability, accuracy

Cons: expenses

Iterative solvers	2D/3D
Memory	$\mathcal{O}(N \log N)$
Time	$\mathcal{O}(N \log N)$

GMRES, FGMRES, BICGSTAB, TFQMR, Conjugated Gradients

Iterations $x_j = F\left(x_0, \dots, x_{j-1}\right)$

End up $e(x_j) < TOL$

Pros: economy

Cons: stability, sensitivity to initial approximation

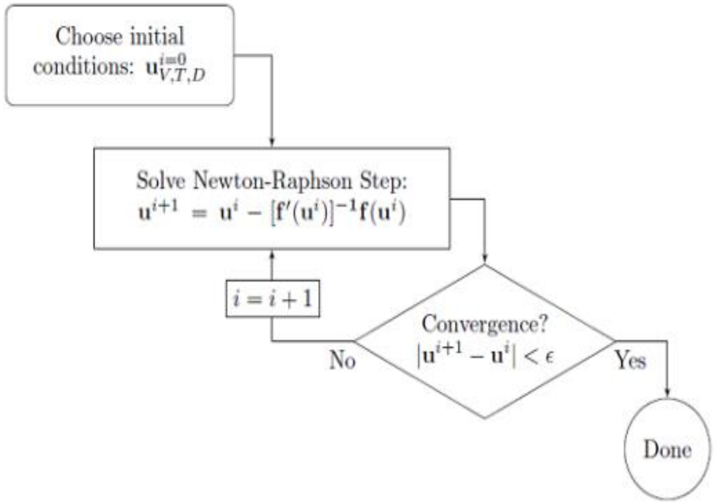

Newton method $\mathcal{L}(U) = 0, \quad U_{j+1} = U_j + \lambda \Delta \mathrm{U}, \quad 0 < \lambda \leq 1$

Stiffness matrix $K = -\mathcal{L}'(U_j), \quad K\Delta U = \mathcal{L}(U_j), \quad U_0$ – initial guess

Solution/Residual Based $err < k \cdot tol, \quad tol \sim 10^{-3}$ ($< 2.22 * 10^{-16}$)

FEM method: solution

Jump of the potential and continuity of the field across thin cut:

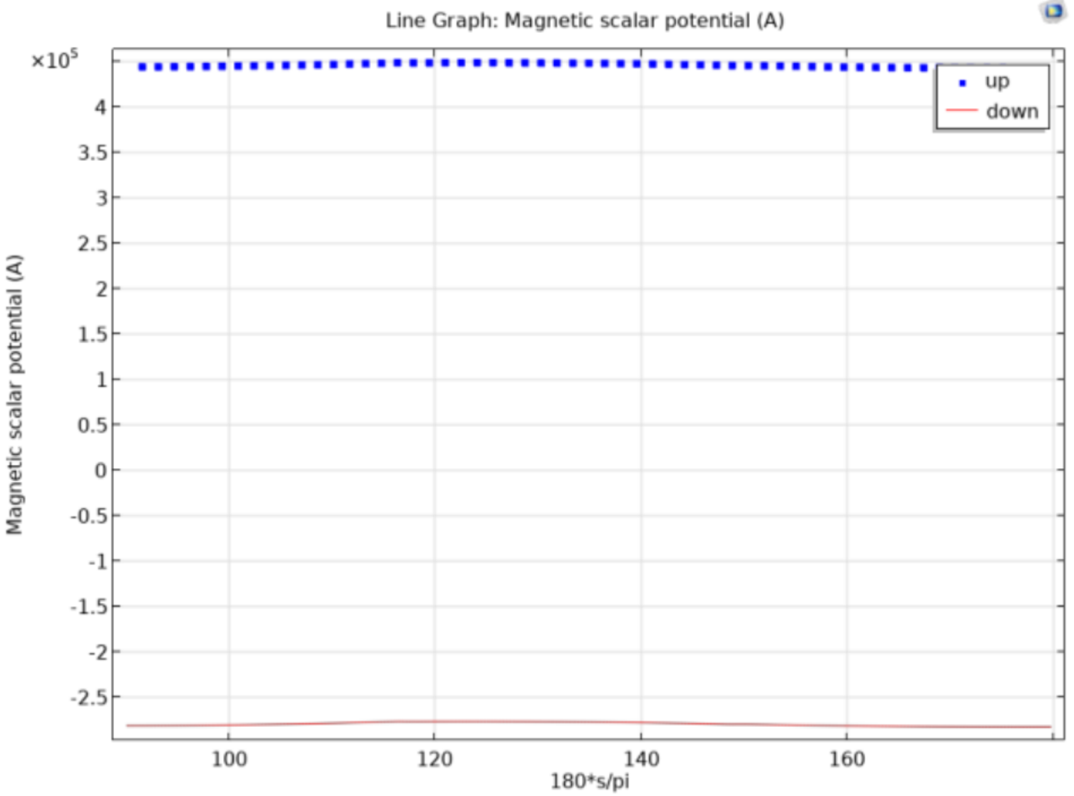

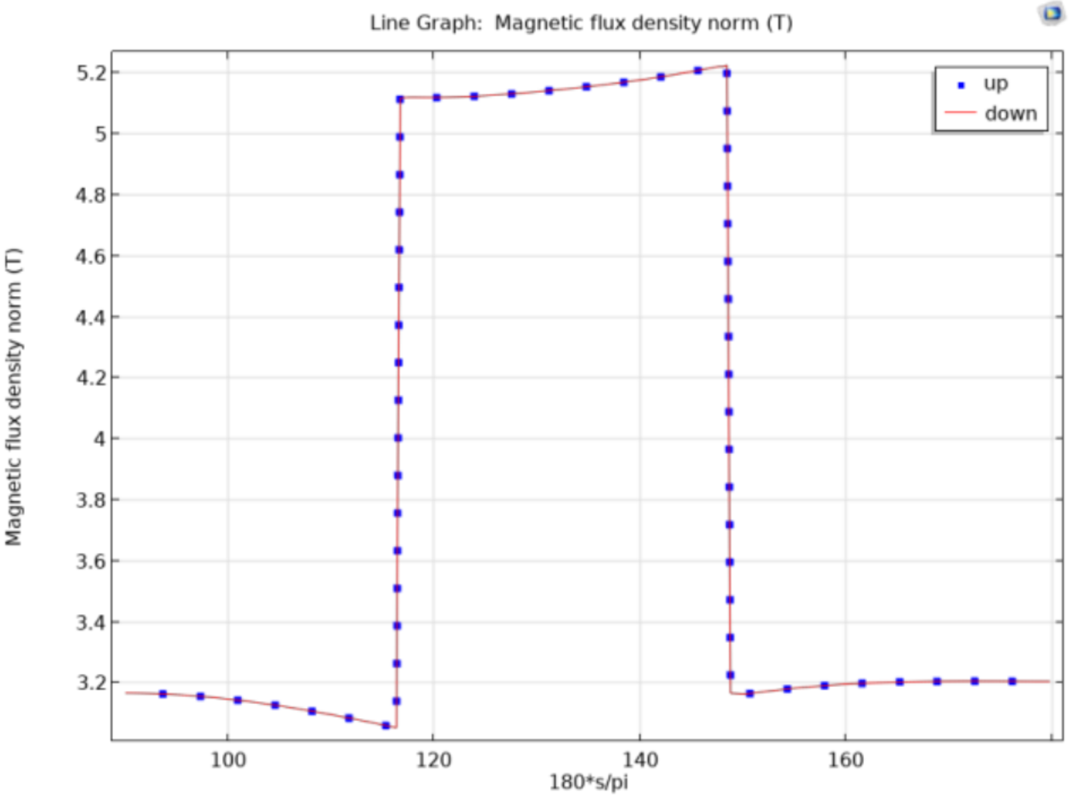

Figure 7: The potential jump and the field continuity across thin cut.

FEM method: solution

Current and field inside the coil:

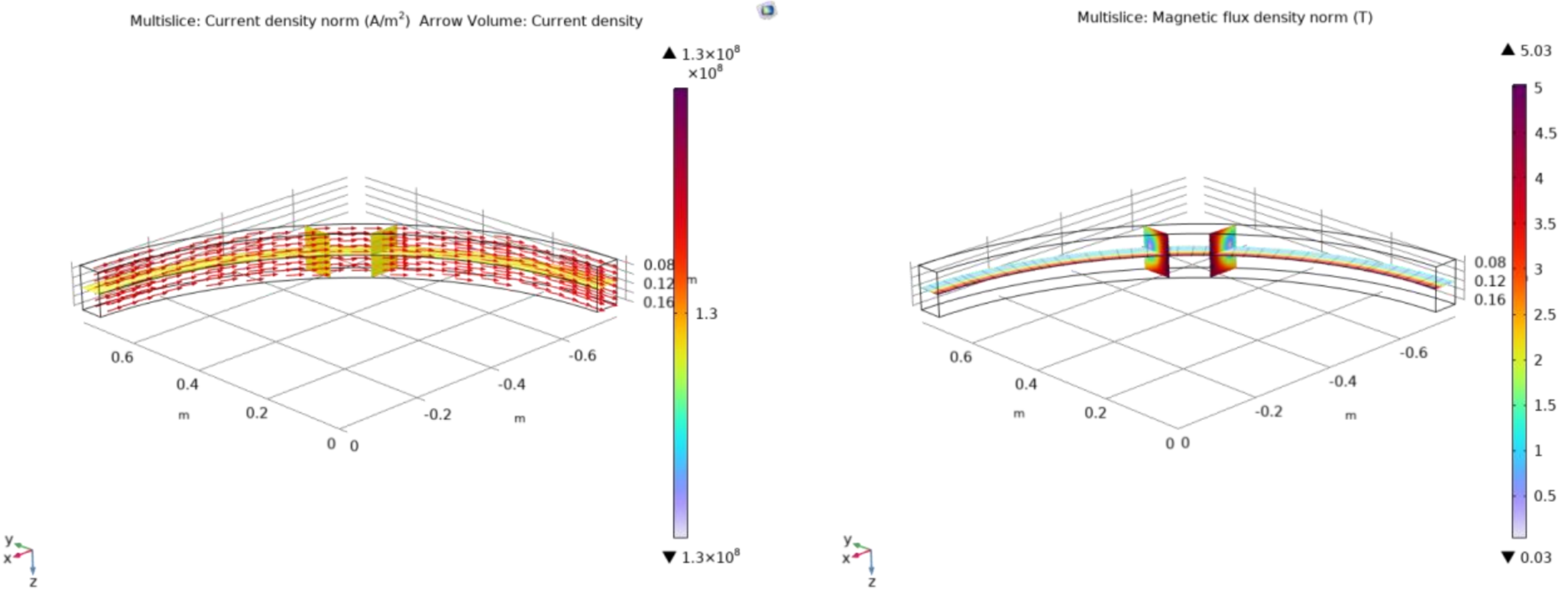

Figure 8: The current and field distributions inside the coil.

FEM method: solution

The field distributions outside conductor:

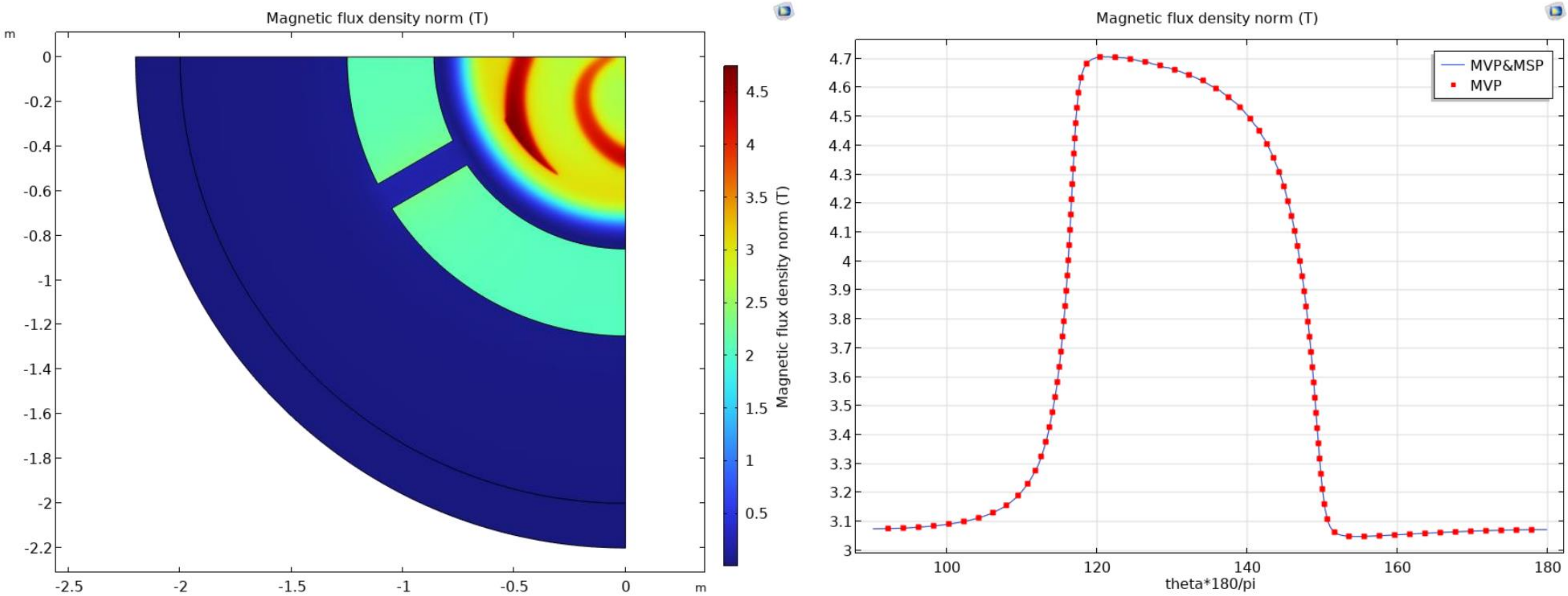

Figure 9: Distributions of the magnetic flux density norm over the median plane (left) and along the azimuthal direction (right). Solid and points refer to calculations with MVP&MSP and MVP formulations, respectively.

FEM method: comparison

Comparison MVP vs MVP&MSP:

Table 1:Summary of formulations used to model dipole magnet.

	Element order	Number of FEs	Number of DOVs	Memory (Gb) Phys/Virtual	Time of computation	Number of iterations
MVP&MSP	3/3	423 198	2 049 396	38.19/56.59	8m 33s	7
MVP	3	414 840	9 958 301	393.15/443.24	4h 12m 46s	8

The reduction of DOFs by a factor of 4.85
The reduction of RAM by a factor of 10
The reduction of time processing by a factor of 30
For relative error between the two of 0.0003 Tesla, or 3 Gausses.

Using exclusively the scalar potential:

- By construction, the MMF of coil is represented by the potential jumps across thin cuts to induce the magnetic fields in the current-free regions;
- Thus, the induction effect of coil on entire problem domain can be modeled by using either thin cuts, or permanent magnets with potential jumps and (de)magnetization defined by the equivalent MMF of the coil;

reproducing coil impact with thin cuts:

Figure 10: Homogenized coil represented by a single cut.

$\Delta V_m = I$

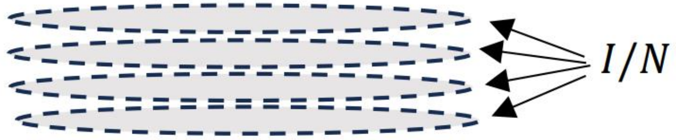

Figure 11: Equivalent multi-wire coil represented by cuts for each wire.

Both are just virtual geometrical objects used solely for modeling of the coil impact.

reproducing coil impact with PMs:

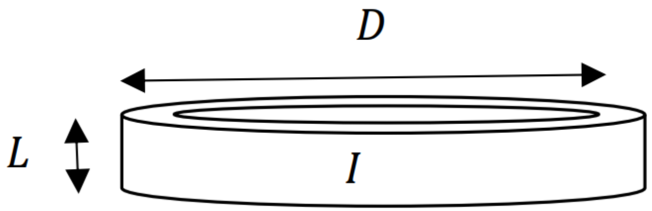

Figure 11: Homogenized coil.

$H_c = {}^{I}/_{L}$

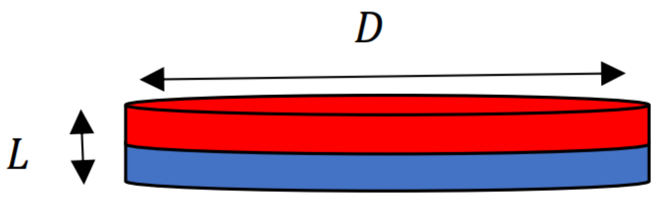

Figure 12: Equivalent permanent magnet.

Using exclusively the scalar potential:

A single model geometry with optimized cut plane and PM to substitute the coil impact.
Both entities are crossing the air gaps and the ferromagnetic sectors.

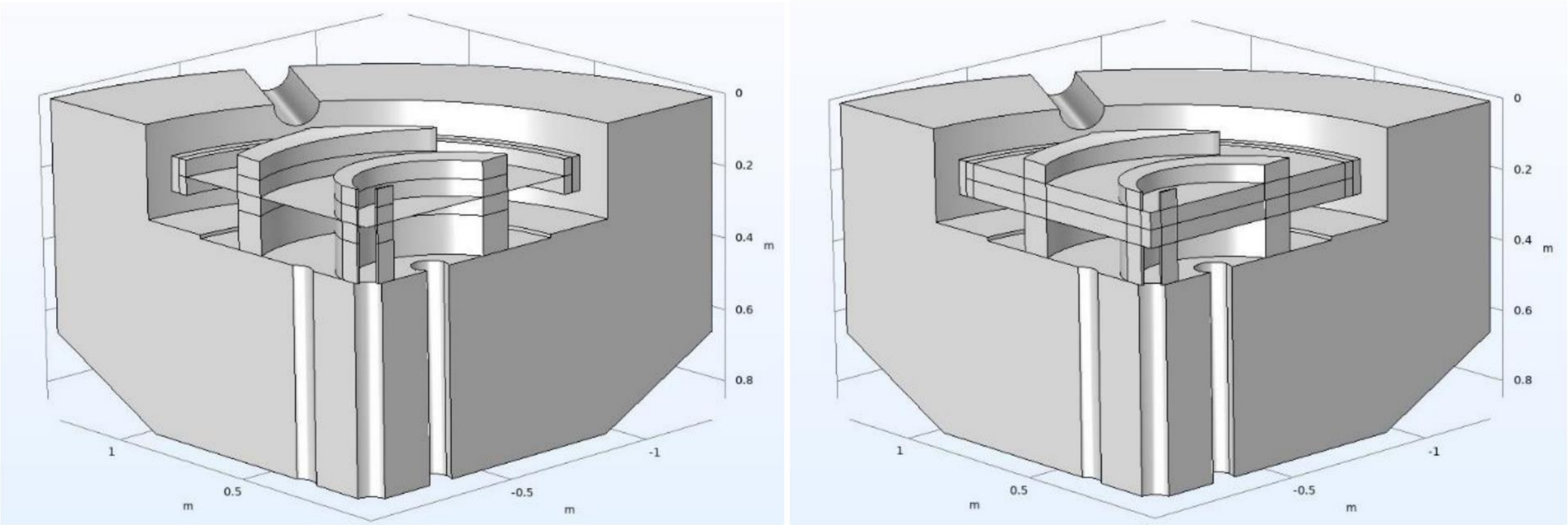

Figure 13: A single model geometry with the cut plane and the PM crossing the air gaps and the ferromagnetic sectors.

Using exclusively the scalar potential:

Cropped geometry with nonlinear BH-curve after introducing PM

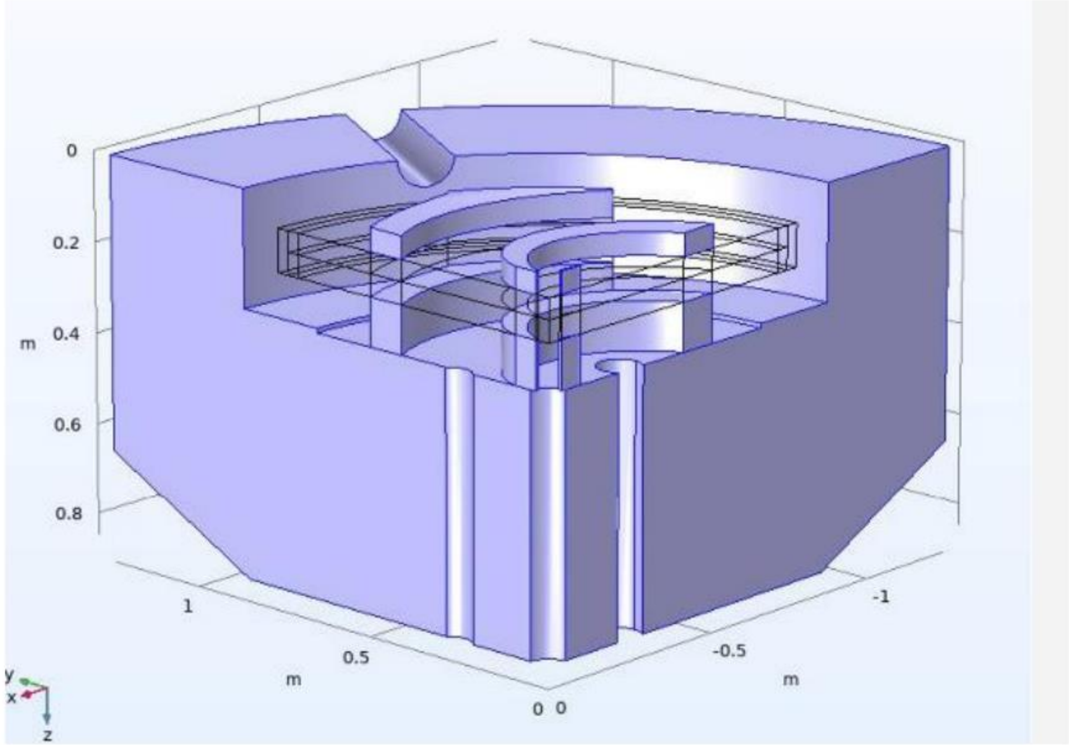

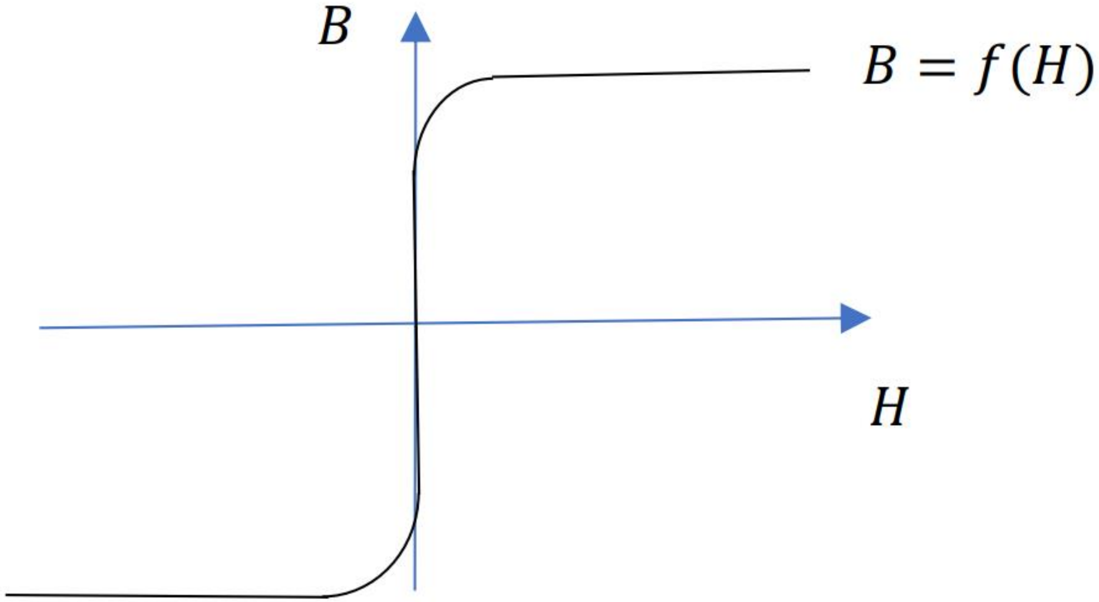

Figure 14: The nonlinear part of the magnetic system after constructing PM.

Using exclusively the scalar potential: virtual PM

The part crossing the air gaps is modeled as the linear PM with almost constant permeabolity specified either by the magnetization $M = \mu_r H_c$, or the remanent flux density $B_r = \mu_0 \mu_r H_c$

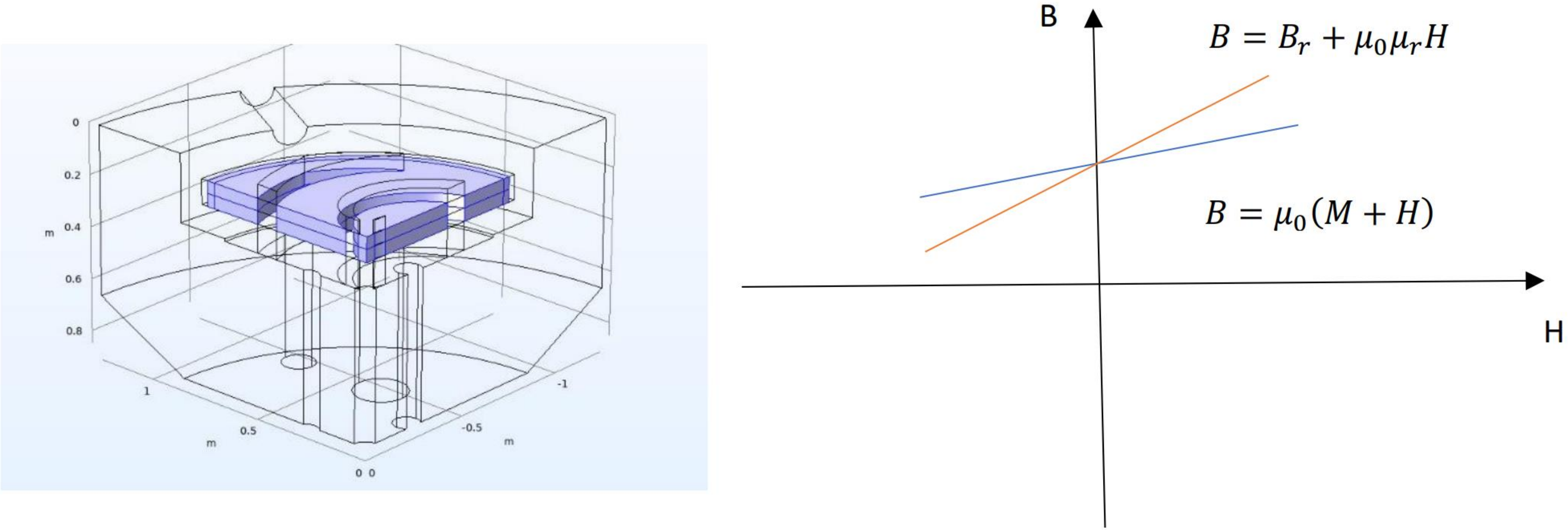

Figure 15: The linear part of the virtual PM specified by either the remanent flux density $\boldsymbol{B_r}$, or the magnetization $\boldsymbol{M}$.

Using exclusively the scalar potential: virtual PM

The part crossing the ferromagnetic sectors is modeled as the nonlinear PM specified by the nonlinear demagnetization BH-curve

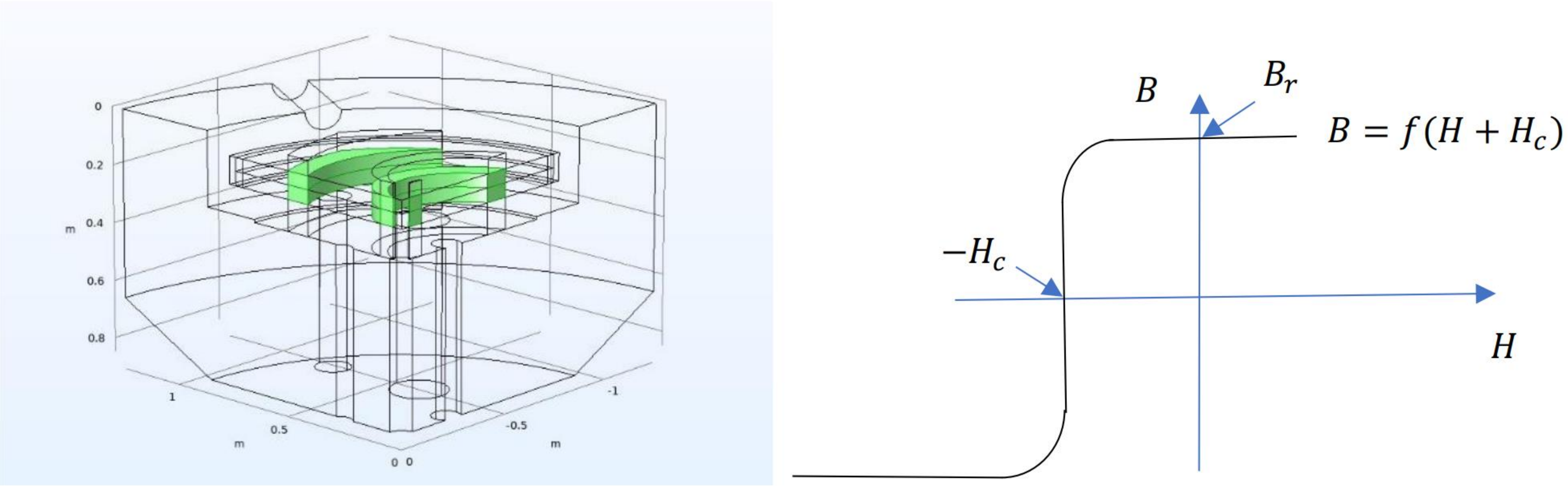

Figure 16: The nonlinear PM specified by the nonlinear demagnetization BH-curve.

Using exclusively the scalar potential: virtual PM

The nonlinear demagnetization BH-curve of PM is obtained via shifting the original BH-curve by a coercivity H_c to the left

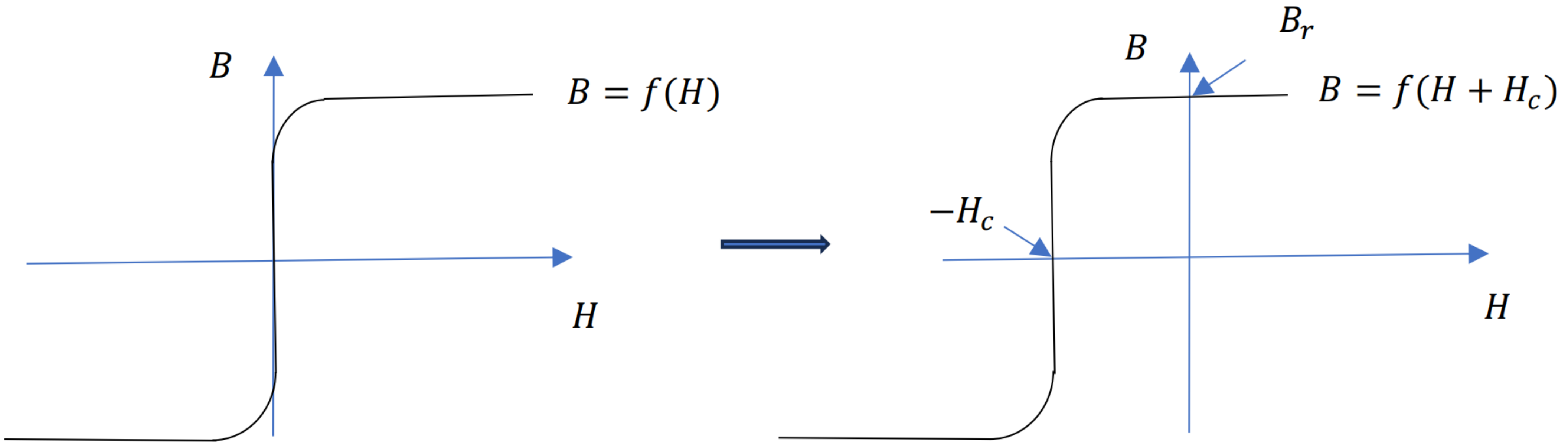

Figure 17: The demagnetization curve of nonlinear PM is obtained via shifting the original BH-curve by H_c to the left. This curve corresponds to a nonlinear material with a remanent flux density $B_r = f(H_c)$ at $H = 0$..

where the coercivity H_c defined from the equivalent MMF of the coil is the value of external field necessary to demagnetize PM.

Using exclusively the scalar potential: FEM modeling

FEM modeling based on three MSP formulations is performed and compared by using a single model geometry of the magnetic system:

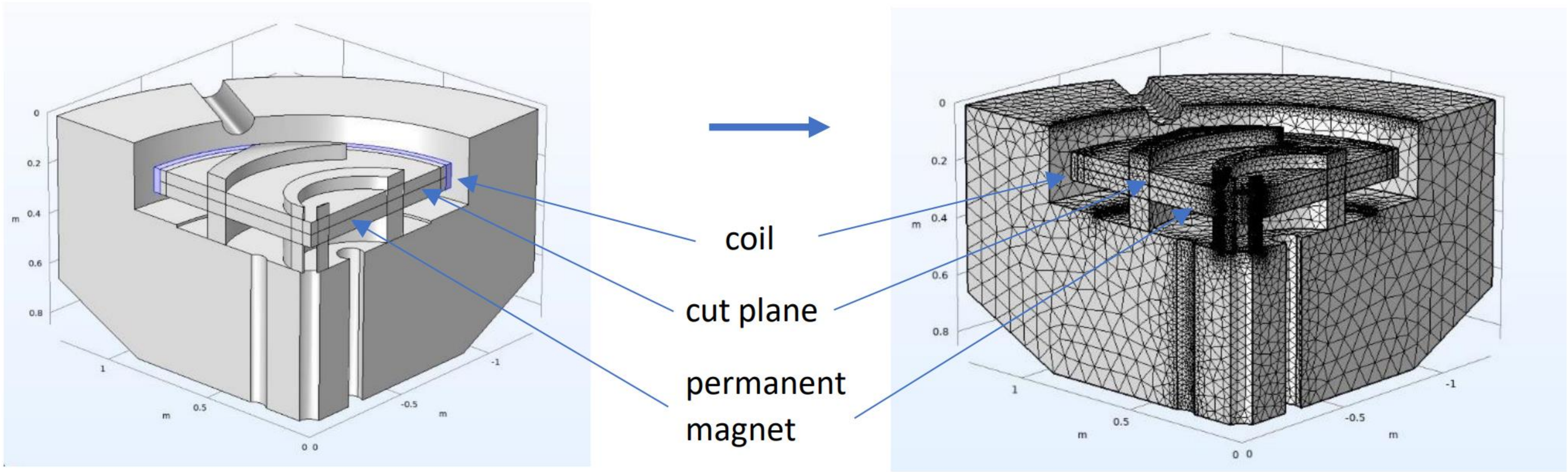

Figure 18: A single geometry for comparison of FEM modeling based on three formulations using scalar potential.

Using exclusively the scalar potential: solution

MSP with cut: field distributions compared to reference field

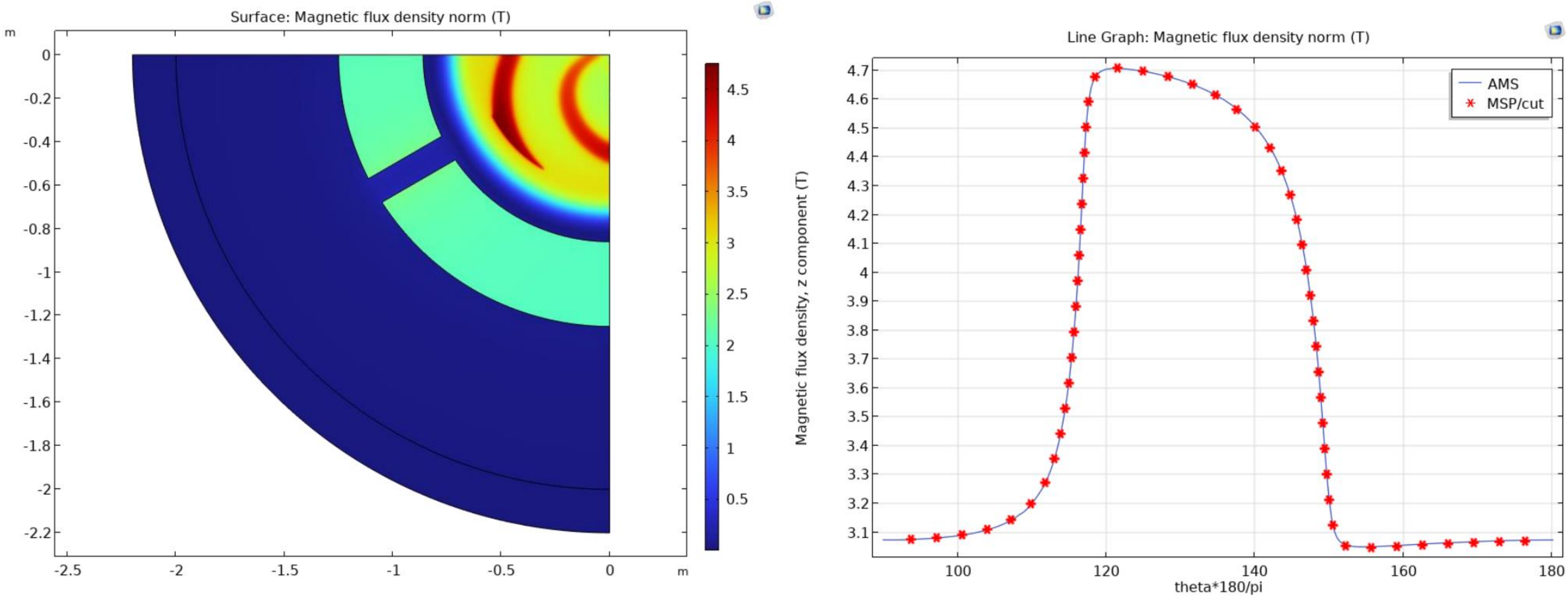

Figure 19: Distributions of the magnetic flux density norm over the median plane (left) and along the azimuthal direction (right). Solid refers to the reference field distribution and points to calculation with MSP/cut formulation.

Using exclusively the scalar potential: solution

MSP/PM and MVP&MSP: fields distributions compared to reference field
Reference solution: iterative $\boldsymbol{A}$-based AMS-solver, run time 21h 2m 33s

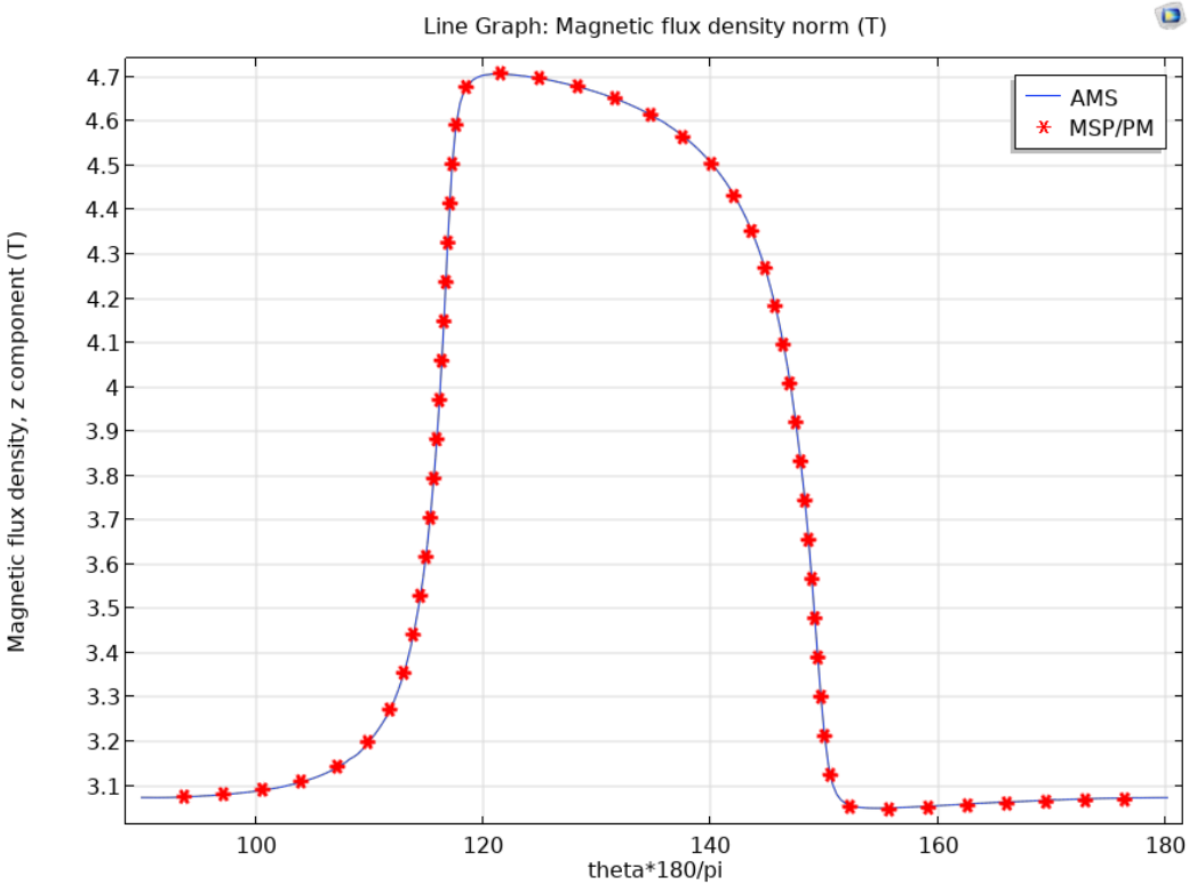

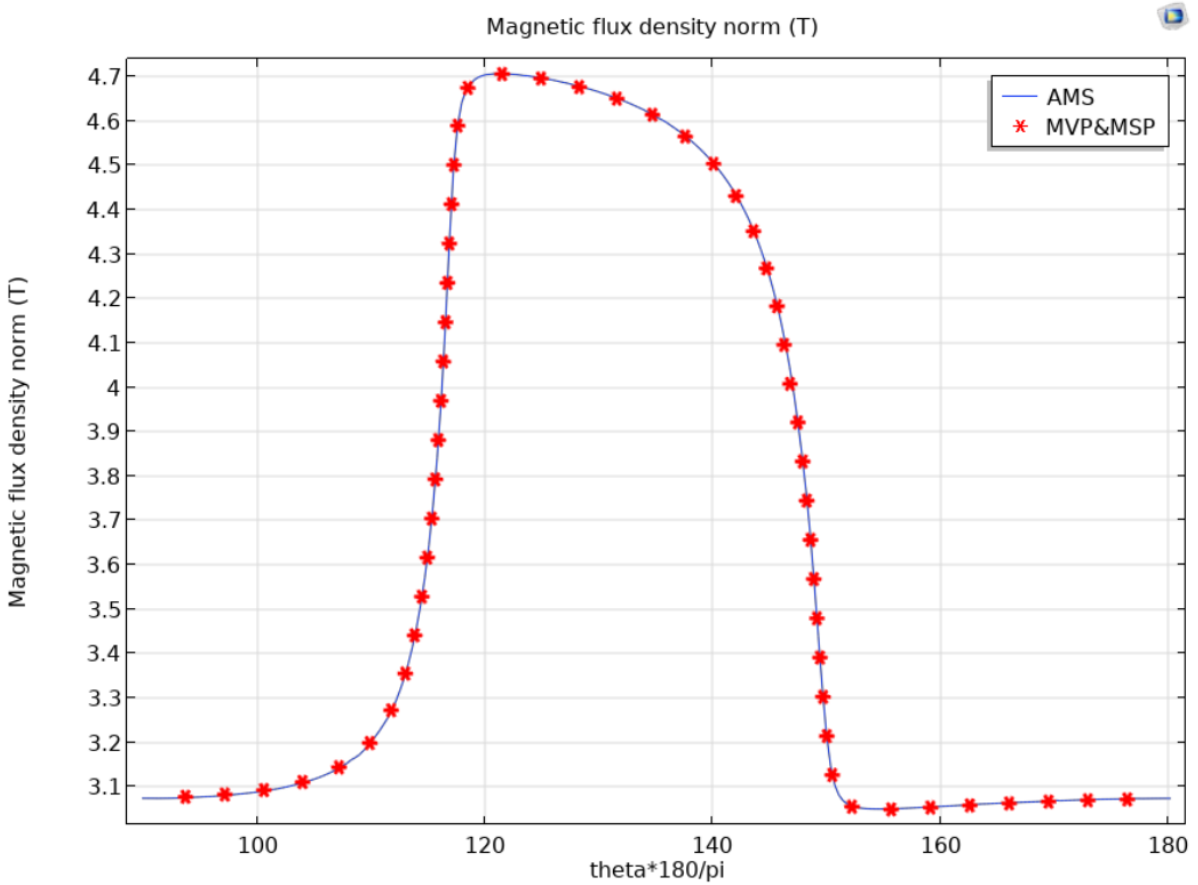

Figure 20: Distributions of the magnetic flux density norm along the azimuthal direction. Solid refers to the reference field distribution and points to calculations with MSP/PM (left) and MVP&MSP (right) formulations.

Using exclusively the scalar potential: comparison

Comparison between three MSP-formulations: MSP/cut vs MSP/PM vs MVP&MSP

Table 2: Summary of MSP-formulations used to model dipole magnet.

	Element order	Number of FEs	Number of DOVs	Memory (Gb) Phys/Virtual	Time of computation	Number of iterations
MSP (cut)	3	779 409	3 635 616	46.39/65.99	14m 31s	8
MSP (PM)	3	779 409	3 635 516	48.04/67.66	14m 13s	8
MVP&MSP	3/3	779 409	3 750 232	77.89/99.8	22m 46s	7
MVP	2	779 409	6 160 618	196.72/226	1h 36m 24s	6

Max error: MVP&MSP 0.0022; MSP (cut) 0.0050; MSP(PM) 0.0028.

Chervyakov A., Finite-element modelling of magnetic fields for superconducting magnets with magnetic vector and total scalar potentials using COMSOL Multiphysics®// Int. J. Engineering Systems Modelling and Simulation. — v.13, 2022-P.117-133;
Chervyakov, A., Comparison of magnetic vector and total scalar potential formulations for finite-element modeling of dipole magnet with COMSOL Multiphysics//physics.comp-ph/arXiv:2107.01957, 2021.

Conclusion:

- The use of magnetic scalar potential allows to substantially reduce the amount of computer memory and computation time at almost similar accuracy for finite-element modeling of the resource-demanding magnetization problems;

- Most efficiently, the MSP-formulations can be utilized for modeling of magnetic systems, where a significant number of simulation runs with significant variation in geometric shapes is required during development of the optimal system design;

- The A-based formulation together with the iterative AMS solver, as providing the excellent quality of computation, can still be useful for the final check-up on the optimized system design;

Acknowledgment:

- To team of JINR Dubna (G.D. Shirkov, G.A. Karamysheva) for involving into developing of a prototype of the isochronous cyclotron for medical application;

- To team of HYBRILIT JINR Dubna (D. Podgainy, O. Streltsova, M. Matveev, D. Belyakov, M. Zuev) for providing the excellent conditions for computations and continuous support;

Thank you for your attention!